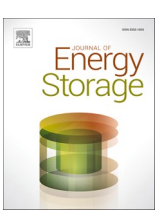
ELSEVIER

Contents lists available at ScienceDirect

# Journal of Energy Storage

journal homepage: www.elsevier.com/locate/est



# Research Papers

# Predicted roundtrip efficiency for compressed air energy storage using spray-based heat transfer

Juliet G. Simpson<sup>a,\*</sup>, Chao Qin<sup>b</sup>, Eric Loth<sup>a</sup>

- a Department of Mechanical and Aerospace Engineering, University of Virginia, 122 Engineer's Way, Charlottesville, VA 22903, United States of America
- b School of Engineering and Computer Science, Washington State University, 14204 NE Salmon Creek Ave, Vancouver, WA 98686, United States of America

# ARTICLE INFO

Keywords:
Compressed air energy storage
Spray cooling
Compression
Expansion
Roundtrip efficiency
Heat transfer

#### ABSTRACT

Compressed air energy storage (CAES) is a low-cost, long-duration storage option under research development. Several studies suggest that near-isothermal compression may be achieved by injecting water droplets into the air during the process to increase the overall efficiency. However, little is known about the thermal-fluid mechanisms and the controlling nondimensional parameters of the expansion process, which has previously been assumed to mirror the compression process. Furthermore, the isothermal round-trip efficiency and the impact of spray-based CAES have not been investigated. This study uses a validated 1-D model for compression and expansion with spray injection to complete a parametric analysis to analyze the thermal-fluid time-dependent physics and resulting roundtrip isothermal efficiency of a CAES system. Comparing the results for compression and expansion simulations, compression is found to have a higher isothermal efficiency than expansion for the same set up. The polytropic index for both compression and expansion tends to decrease and approach the ideal isothermal limit as nondimensional mass loading increases and as nondimensional Crowe number (ratio of thermal response time to domain time) decreases. As such, the highest efficiency designs are those with slow compression speeds and high spray flow rates to achieve high mass loading and those with small droplets to achieve low Crowe numbers—as long as spray work is neglected. If spray work is included, the optimum spray conditions shift to those with lager drop sizes. For example, roundtrip isothermal efficiency peaks around 95 % at a mass loading of 14 and at Crowe numbers < 0.1 with a pressure ratio of ten. The results indicate that nearisothermal CAES compression and expansion is possible but that spray work should be included for significant mass loadings (e.g. greater than unity). Further investigation is recommended to consider effects of multidimensionality, turbulence, wall-interactions, and droplet dynamics.

# 1. Introduction

Inexpensive, long-duration energy storage options are needed to meet electrical demand as an increasing share of electricity comes from renewable sources. Currently, dispatchable fossil fuel generation or overbuilding renewable generation are often more economical solutions than long-duration energy storage with Lithium-Ion batteries, so other energy storage options are increasingly important. Compressed air energy storage (CAES) has strong potential as a low-cost, long-duration storage option, but it has historically experienced low roundtrip efficiency [1]. The roundtrip efficiency is determined by the thermal losses, which tend to be large during the compression and expansion processes, and other losses (such as mechanical and fluid friction) which tend to be smaller. CAES has the potential for many novel applications that pair it

with energy storage with renewable energy generation [2,3] or reuse other structures like abandoned mines [4]. Additionally, recent work on using porous rock formations for compressed air storage [2,5], rather than creating expensive pressure vessels, may help increase its deployment.

Isothermal compressed air energy storage (ICAES) utilizes increased heat transfer during the compression and expansion processes to reduce temperature change in the compressed air and increase the overall isothermal efficiency of the process. If air can be compressed at a constant temperature, then all of the work input goes into compression rather than heat generation, and thus there is a potential to retrieve all of the input work during the expansion process. One option for achieving near-isothermal air compression and expansion is by injecting water droplets during the process. The spray injection has a large thermal mass and can absorb heat from the air during compression and transfer heat to

E-mail address: js9sw@virginia.edu (J.G. Simpson).

<sup>\*</sup> Corresponding author.

Nomer	nclature	$U_{ m piston} \ V$	Piston speed $(m/s)$ Volume $(m^3)$
ρ	Density (kg m <sup>-3</sup> )	W	Work (W)
•	Ratio of specific heats of air	$w_{\text{term}}$	Droplet terminal relative velocity (m/s)
γ	Isothermal efficiency	z term	Position (m)
η τ	Time constant (s)	۵	rosition (m)
		Subscrip	ts
$c_p$	Air specific heat capacity at constant pressure (J kg $^{-1}$ K $^{-1}$ )	1	Beginning of process
$c_s$	Water specific heat capacity at constant pressure	2	End of process
	$(J kg^{-1} K^{-1})$	a	Air
$c_{\nu}$	Air specific heat capacity at constant volume ( $J kg^{-1} K^{-1}$ )	atm	Atmospheric
Cr	Crowe number	avg.	Average
d	Droplet diameter (m)	С	Compression
D	Cylinder diameter (m)	CR	Critical
k	Air thermal conductivity (W $m^{-1}$ K <sup>-1</sup> )	cyl	Cylinder
L	Vertical length from cylinder head (m)	ď	Droplet
m	Mass (kg)	D	Domain
ML	Mass loading	Е	Expansion
n	Polytropic index	fall	Fall
Nu	Nusselt number	init	Initial
P	Pressure (Pa)	iso	Isothermal
$\Delta P$	Overspray pressure (Pa)	RT	Roundtrip
PR	Pressure ratio	spray	Spray
$q_{ m spray}$	Spray flow rate $(L/s)$	T	Thermal
T	Temperature (K)	tot	Total
t	Time (s)	101	2000

the air during expansion.

For a CAES system, the physics of the thermal and fluid interaction as well as the overall isothermal roundtrip efficiency of the process are important to understand how much of the energy put into storage can be recovered for later use and to design a system for grid-scale energy storage.

CAES can use multiple types of compressors, but reciprocating compressors are common for isothermal CAES, either using a solid/mechanical piston or a liquid piston. One benefit of reciprocating compressors is the ability to use them both for compression and expansion, cutting the equipment costs in half. Roundtrip efficiency is critical to a CAES design, and if the same equipment is used for both compression and expansion, then it is important to consider isothermal roundtrip efficiency early in the design process. Liquid piston roundtrip efficiency varies and was found to be 78 % for a pressure ratio of 39 by Hu et al. [6]. Some unique CAES designs that utilize spray cooling have found that adding water spray increased roundtrip efficiency [7,8].

Both experimental and computational work has been previously completed to investigate near-isothermal CAES, including studying liquid piston compression [9,10] and heat transfer inserts [11,12], with the primary emphasis on the compression portion (rather than on the expansion portion or on the entire roundtrip process). However, few studies have considered the performance of a matched compression and expansion system for a standard compressed air energy storage system, where the system parameters are the same for both, and no experimental results have been reported. Compression and expansion are not identical processes, for a non-isothermal process, so the same system set up will have different efficiencies for compression and expansion even if the same system parameter are employed. Optimizing for a roundtrip system is critical when designing a near-isothermal CAES system for longduration storage and may give different results than optimizing for either compression or expansion individually. Thus, there exists a need for further study of roundtrip isothermal CAES systems.

Experimental work by Wieberdink et al. [13] and Yan et al. [14] looked at liquid piston near-isothermal compression and expansion cases, both with and without porous media inserts (but with no spray

injection), for small-scale systems. They found that piston speed had a large effect on efficiency, where slower piston speeds resulted in processes closer to isothermal for both compression and expansion. Notably, the temperature and pressure plots from these studies showed different trends for compression and expansion processes. While a fully-isothermal process would look the same for compression and expansion, the real processes as measured by Wieberdink et al. and Yan et al. showed differences. In particular, the temperature during compression exhibited a relatively monotonic increase and the pressure rose at a nearly constant rate with time. However, the temperature during expansion showed both increases and decreases while the pressure slope over time was inconsistent. As such, the expansion process was not as easily characterized and is less understood.

Several studies have sought to understand the thermodynamics for spray-based compression with experiments and simulations. Experiments on spray-cooled compression with a liquid piston were reported in Patil et al. [15]. Previous work on modeling spray-cooled compression has included 1-D droplet heat transfer modeling by Qin & Loth [16], Sapin et al. [17], and Simpson et al. [18], which document an increase in isothermal compression efficiency with increasing spray mass loading and with decreasing drop size, though spray work effects were not considered. These simulations did not include spray-based expansion, so no round-trip efficiency predictions were available.

While extensive research has been completed on near-isothermal compression, it is critical that both compression *and* expansion be modeled to understand the full roundtrip system for CAES. However, the thermodynamics of the expansion process for spray-based CAES has been less studied. In particular, there are no published experimental data on spray injection expansion, which remains an area of critical interest to assess the viability of spray-based CAES. However, some researchers have modeled expansion with spray-injection. Yu et al. [19] modeled a generally complete expansion system including orifices, nozzles, and the motion of the piston while injecting high-temperature water mist during expansion. However, the model was only applied for one specific spray case, so no parametric influences could be identified. Zhang et al. [20] simulated spray-injection during expansion and

varied the injected mass loading, finding that spray heat transfer increased the expansion work production by 16 % over adiabatic expansion. However, these studies did not vary cylinder dimensions, compression parameters, or droplets sizes, and thus were not able to identify the most important parameters for high-efficiency expansion.

Additionally, the work of injecting spray during the compression and expansion processes may be significant. Experiments by Patil et al. [15] reported both compression work and spray work, separately, and they found that spray work could approach the magnitude of compression work, thus offsetting the heat transfer benefits. Furthermore, while initial increases in spray pressure resulted in large temperature abatement, larger increases in spray pressure provided only marginal temperature reductions due to spray heat transfer [15]. In simulation studies, increasing the spray pressure (and thus increasing flow rate and decreasing droplet size) also reduced temperature rise during compression, but the increased spray pressure must be balanced against the increased spray work which can negatively affect efficiency [15,21-23]. Finally, Odukomaiya et al. [7] predicted a peak and then drop off in roundtrip efficiency with increasing spray mass loading, though they did not consider the effect of droplet size. Thus, it is important to consider the impact of spray work when using spray injection for both compression and expansion.

Odukomaiya et al. [7] modeled a roundtrip compression and expansion system with spray injection and a liquid piston and did compare multiple different droplet sizes and spray flow rates, giving some initial insight into the influence of important parameters on roundtrip efficiency. The work herein attempts to focus specifically on the spray-based heat transfer effects using fundamental theory, the key nondimensional parameters, and a wide variety of dimensional scales to understand the key thermodynamics of the compression and expansion processes, including the relative importance of spray work to isothermal efficiency. While most experimental work on spray-cooled compression has been completed with small-scale pistons, we expect that utility scale energy storage will involve much larger pistons where droplet surface area is significantly larger than wall surface area.

The main contribution of this paper is to complete a parametric analysis of compression and expansion processes with spray injection using a validated 1-D model to analyze the thermal-fluid physics and roundtrip isothermal efficiency of a CAES system. Importantly, this paper shows significant differences between compression and expansion thermodynamic processes and discusses how those may affect isothermal roundtrip efficiency. This paper also identifies high-efficiency designs for spray-injection systems with different droplet sizes, both with and without spray work considerations, which will be important for designing long-duration energy storage systems.

This is the first paper to the authors' knowledge to investigate the detailed thermodynamics and heat transfer for the expansion process of a compressed air energy system, and the first to consider a wide variety of conditions. In addition, it is the first to complete a parametric analysis of roundtrip performance by modeling matched pairs of compression and expansion cases. Importantly, this is the first paper to identify the mass loading and the Crowe number as the key thermodynamic controlling parameters for round-trip efficiency. Furthermore, it is the first to show that isothermal efficiency for both compression and expansion can be theoretically predicted in the thermal equilibrium limit and that this theory matches reasonably well with validated simulations for very small droplets. Finally, this is the first work to consider the competing effects of spray work and spray heat transfer for a variety of pressure ratios, drop sizes and mass loadings. Thus, it fills an important gap in the literature by looking at the full roundtrip system, as would be needed to implement CAES.

#### 2. Methodology

# 2.1. Physics and geometry of numerical model

The system considered herein involves first-stage air compression or expansion in a cylinder with direct water spray injection. The simulations consider only heat transfer between the air and the droplets (sidewalls and top and bottom surfaces are assumed to be adiabatic). As such the results directly investigate spray-based effects and are applicable for either water (liquid piston) or solid piston systems (since the piston surface is assumed to be flat and provides no heat transfer) Heat transfer to the walls and piston are not included herein since the focus is on utility-scale pistons where droplets are expected to be the driving source of heat transfer and because previous parametric sweeps in Ref. [18] calculated that the droplet surface area was 10-100 times larger than the other surface areas for moderate piston sizes. The model considers 1-D droplet motion along the z-axis, which starts at the top center of the cylinder, as seen in Fig. 1 The 1-D model for compression builds upon work by Oin & Loth [16] and Simpson et al. [18], and was extended to consider expansion process. It assumes inert droplets within laminar air flow with one-way coupling between the air and droplets and no multi-dimensional or wall interactions.

The compression and expansion processes are simulated with a twostep procedure. In each timestep, first the air volume is changed adiabatically and then heat transfer is allowed between the air and the droplets. The temporary air temperature  $(T^{'})$  in-between the time steps (i) is calculated as

$$T_{a}^{'i+1} = \left(\frac{V^{i}}{V^{i+1}}\right)^{\gamma-1} T_{a}^{i}$$
 (1)

Then heat transfer is allowed between the droplets and the air and is summed over all the droplets, resulting in a final air temperature and pressure for that timestep.

$$Q_{tot} = \sum \pi dk_{\rm a} Nu \left( T_{\rm a}^{i+1} - T_{\rm d,j}^{i} \right) \tag{2a}$$

$$T_{\rm a}^{i+1} = T_{\rm a}^{i+1} - \frac{Q_{\rm tot}dt}{m_{\rm a}c_{\nu}}$$
 (2b)

$$P^{i+1} = \frac{m_a R T_a^{i+1}}{V^{i+1}} \tag{2c}$$

where j is the droplet index, d is the droplet diameter, k is the air thermal conductivity, Nu is the Nusselt number, and m is the mass. Further details on the 1-D model are provided in Simpson et al. [18], where the model was validated against experimental results.

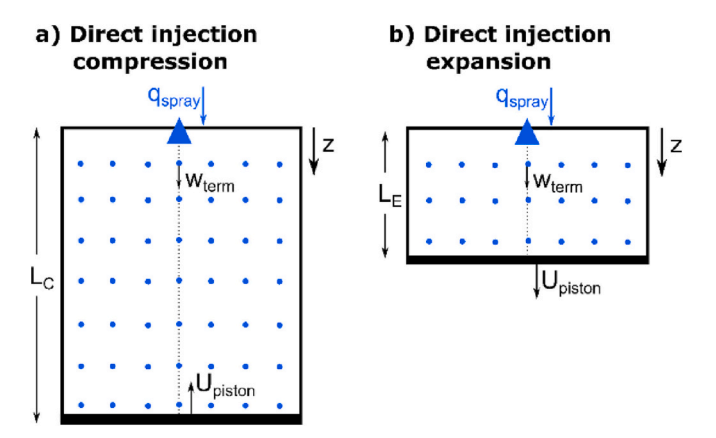


**Fig. 1.** Notional schematics of direct injection spray at the beginning of each piston motion (after air has entered the chamber with initial spray injection): a) compression and b) expansion.

A single spray nozzle was used for the cylinder and cylinder lengths were chosen to vary from 10 to 50 cm. The compression cylinders were all fixed at a diameter of 10 cm, which is consistent with previous experiments and allowed a single nozzle to reasonably provide relatively high mass loading without having most of the spray impact the sidewalls. A full-scale system would generally have a much larger diameter and include many nozzles. However, the 1-D aspects of such a full-scale system can be approximated with the present single-nozzle system since sidewall effects are neglected, so long as the number of nozzles scales with the increase in cross-sectional area (so mass loading is held constant).

For all simulations, the piston speed ( $U_{\rm piston}$ ), total cylinder length ( $L_{\rm cyl}$ ), water volumetric spray flow rate ( $q_{\rm spray}$ ), droplet diameter (d), and maximum pressure ratio (PR) are prescribed. For simplicity, the piston speed is a constant within a given simulation, which is representative of a liquid piston compression process. Notably, this may give different results than sinusoidal piston speed profiles that are typical of solid, mechanical pistons.

In a complete compressed air energy storage system, the air would enter and leave the cylinder through valves and incur frictional and aerodynamic losses in piping and storage losses. However, for simplicity in this assessment, only the compression and expansion process are considered. As such, major and minor losses from valves, fittings, and piping are not included, and a constant pressure storage system is assumed (such as an open accumulator).

For compression, the cylinder starting length ( $L_C$ ) is prescribed as the total cylinder length,  $L_1=L_C=L_{\rm cyl}$ . Before the compression process, air at atmospheric pressure ( $P_{\rm atm}$ ) and room temperature is drawn into the cylinder during the "draw in" process. The cylinder starts at an initial volume and atmospheric pressure, and it compresses until the target critical pressure is reached. The critical pressure ( $P_{\rm CR}$ ) can be defined as

$$P_{\rm CR} = PR^*P_{\rm atm} \tag{3}$$

The process to push the air out at constant pressure is not simulated and is instead determined using boundary work theory. In reality, the air may be pushed out into the next stage or a storage vessel.

In expansion, the air starts at the critical pressure at cylinder length  $L_{\rm E}$  and is expanded until it reaches the final atmospheric pressure. The initial expansion cylinder length is defined based on an isothermal process, where the starting cylinder length  $(L_{\rm E})$  can be related to the total cylinder length  $(L_{\rm cyl})$  and the pressure ratio as follows, given that the volume of an isothermal, ideal gas is inversely related to the pressure

$$L_1 = L_E = \frac{L_{\text{cyl}}}{PR} \tag{4}$$

Thus,  $L_{\rm E}$  is the length that the piston moves during the draw-in process when high pressure air is drawn into the cylinder at constant temperature and pressure while droplets are sprayed into the cylinder, and  $L_{\rm cyl}$  is the maximum expected length of the cylinder at the end of the expansion process (as an isothermal process is the longest possible process).

The water droplet spray would have a range of droplet sizes and would take time to disperse from the injection site and fill the chamber fully. Herein the droplets are modeled using a single size, the Sauter mean diameter, to simplify the simulations and focus on the fundamental effect of drop size on efficiency. In actual sprays, there would be a range of droplets (some smaller and some larger than the Sauter mean diameter) and a corresponding a range of terminal velocities and heat transfer rates. Only modeling the droplets in 1-D accounts for the time to disperse in the z-direction but does not account for radial dispersion of droplets within the chamber.

The water droplets are sprayed in at a constant flow rate from the top of the chamber during the draw-in process and during the compression/expansion process, until the desired pressure is reached. The droplets are sprayed in at the same volumetric flow rate during the draw-in process

for both compression and expansion. Note that at constant piston speed, the draw-in process takes longer for compression due to the longer starting cylinder length ( $L_{\rm C} > L_{\rm E}$ ), and thus more droplets are sprayed in initially for compression than expansion, as illustrated nominally in Fig. 1 where the compression schematic has more droplets in the chamber at the beginning of the process than the expansion schematic. The droplets are sprayed in at a temperature of 300 K.

The drop Reynolds number, relative terminal velocity, and drag coefficient are found iteratively, based on White's drag coefficient, which is appropriate for drop Reynolds number up to 1000 [24]. Droplet velocity is then the sum of the relative terminal velocity ( $w_{\text{term}}$ ) of the droplet and the local air velocity. The air in the cylinder is assumed to have a linear velocity profile, from the moving piston surface to the stationary cylinder top.

The air in the cylinder is assumed to have uniform pressure, temperature, and density and is assumed to obey the ideal gas law. The starting air temperature for all simulations is room temperature (300 K), assuming there is sufficient time between cycles for the air to return to room temperature.

Heat transfer from the air to the droplets is assumed to be the dominant form of heat transfer, and thus the piston and walls are considered adiabatic and heat transfer is only allowed to the droplets. Heat transfer between each droplet and the air is calculated and then summed to find total heat transfer with the air. Droplet evaporation, boiling, and freezing were not included in the simulations as droplet temperatures are intended to stay between the freezing and boiling points of water. Processes with high isothermal efficiency, as sought by this study, would not experience extreme droplet temperatures, so those effects were excluded for simplicity. Additionally, an anti-freeze compound could be added to lower the droplet freezing temperature if needed.

Droplet mass transfer effects from condensations and evaporation have been neglected in previous studies [18–20,25,26], including Ref. [25] which assumed the large mass of injected water droplets would quickly saturate the air and cause little change in droplet diameters. Ref. [18] noted that at the given initial temperature and pressure, a maximum of  $ML \sim 0.02$  would fully saturate the air and additional water mass could not evaporate. However, mass transfer is recommended for future study for cases with ML < 2 and d < 50 µm, as the effects of evaporation are expected to have a more significant impact on the overall process efficiency.

The numerical method employs a two-step process for each timestep, where first the air is compressed or expanded adiabatically, and then heat transfer is allowed between the air and the droplets. This will be time-accurate if temperature changes are small, i.e. the timesteps are small compared to the time for compression and expansion and to the thermal inertia of the drops [25]. Other numerical constraints were added to ensure numerical consistency and convergence. In particular, a simulation result was removed from the dataset if any of the following occurred:

- $\bullet$  There were <100 steps in the simulation (potentially inadequate temporal discretization for accuracy),
- $\bullet$  Droplet momentum response time ( $\tau_p$ ) was >10 % of the total stroke time (terminal velocity assumption may not be valid),
- Piston speed exceeded  $\frac{U_{\text{piston}}}{t_{\text{iso}}} < 0.1g$  (ensuring that if this system was implemented with a real piston, the speed and acceleration would be physically realistic),
- The added water droplet volume at a time step was >50 % of the change in piston volume (the majority of the change in air volume should come from piston motion), or
- More than 10 % of the initial volume of initial volume was droplets (the initial draw-in spray should not significantly change the cylinder volume).

#### 2.2. Outputs and nondimensional parameters

The compression and expansion processes can each be quantitatively characterized in terms of their principal work, isothermal efficiency, and polytropic index.

The compression work is divided into two periods: i) compression occurs from initial atmospheric pressure ( $P_{\rm atm}$ ), starting cylinder length ( $L_{\rm C}$ ), and initial volume ( $V_{\rm 1C}$ ) to the final critical pressure ( $P_{\rm CR}$ ) and final volume ( $V_{\rm 2C}$ ), and then ii) the air is pushed out of the cylinder while maintaining the final pressure. Note that  $P_{\rm 1C}=P_{\rm atm}$  and  $P_{\rm 2C}=P_{\rm CR}$  for compression, but the pressure terms are used herein since they are fixed for each simulation for both compression and expansion, while the volume terms vary. The final pressure is set as the critical pressure, and the final volume and final time are dependent on the compression process and correspond to when the critical pressure is reached (adiabatic compression has the shortest piston travel to achieve  $P_{\rm CR}$ , while isothermal compression needs the longest piston travel). The total work is thus calculated as

$$W_C = \int_{V_{1C}}^{0} (P - P_{\text{atm}}) dV = \int_{V_{1C}}^{V_{2C}} (P - P_{\text{atm}}) dV - (P_R - P_{\text{atm}}) V_{2C}$$
 (5)

Note that compression work is negative because work is put into the system.

The efficiency of the compression process is measured by the ratio of work for an isothermal process to the work for the given process, where the initial (atmospheric) pressure, initial temperature, and critical pressure are all fixed. The isothermal efficiency can thus be written as follows, adapted from [16,27].

$$\eta_{\rm iso,C} = \frac{\left[ \int_{V_{\rm IC}}^{V_{\rm 2C,iso}} (P - P_{\rm atm}) dV \right]_{\rm iso} - (P_{\rm R} - P_{\rm atm}) V_{\rm 2C,iso}}{\int_{V_{\rm IC}}^{V_{\rm 2C}} (P - P_{\rm atm}) dV - (P_{\rm R} - P_{\rm atm}) V_{\rm 2C}}$$
(6)

For a fully isothermal process  $\eta_{\rm iso}=$  1. To minimize work lost due to heat, it is desired that this isothermal efficiency be as close to unity as possible.

If the compression process is treated as a polytropic process, it can be quantified with a uniform polytropic index (n). A polytropic process obeys the following relationship.

$$PV^n = \text{constant}$$
 (7)

For an adiabatic process on an ideal gas, the polytropic index is the ratio of specific heats, i.e.  $n=\gamma=1.4$  for air. For an isothermal process, n=1. For a process with finite heat transfer, n may vary with time during the process due to variations in heat transfer, but the overall average polytropic index  $(n_{\rm avg})$  will lie between these bounds such that  $1 < n_{\rm avg} < \gamma$ . In this case, the average polytropic index for a compression process can be computed by setting the total compression work (Eq. (5)) equal to the equivalent average compression work which assumes a constant polytropic index.

$$W_{\text{avg,C}} = \frac{n_{\text{avg}}}{n_{\text{avg}} - 1} P_{\text{atm}} V_{1C} \left( 1 - P R^{\frac{n_{\text{avg}} - 1}{n_{\text{avg}}}} \right)$$
 (8)

The average polytropic index thus reflects a process that would require the same work to reach a given pressure ratio (PR), starting from the same initial volume and pressure. For high isothermal efficiency, it is desired that n be as close to unity as possible.

The expansion work occurs in two periods: i) air is drawn into cylinder at constant pressure, and then ii) air is expanded from the critical pressure ( $P_{\rm CR}$ ), initial cylinder length ( $L_{\rm E}$ ), and initial volume ( $V_{\rm 1E}$ ) to the final pressure ( $P_{\rm atm}$ ) and volume ( $V_{\rm 2E}$ ). The final volume and time are dependent on the expansion process. The total expansion work can be calculated as

$$W_E = \int_0^{V_{2E}} (P - P_{\text{atm}}) dV = \int_{V_{xE}}^{V_{2E}} (P - P_{\text{atm}}) dV + (P_{CR} - P_{\text{atm}}) V_{1E}$$
 (9)

Note that expansion work is positive because work is moving out of the system.

The efficiency of the expansion process is measured by the ratio of work for the given process to the work for an isothermal process, where the initial pressure, initial temperature, and final pressure are all fixed. The isothermal expansion efficiency can thus be written as

$$\eta_{\rm iso,E} = \frac{\int_{V_{\rm IE}}^{V_{\rm E}} (P - P_{\rm atm}) dV + (P_{\rm CR} - P_{\rm atm}) V_{\rm IE}}{\left[\int_{V_{\rm IE}}^{V_{\rm 2E,iso}} (P - P_{\rm atm}) dV\right]_{\rm iso} + (P_{\rm CR} - P_{\rm atm}) V_{\rm IE}}$$
(10)

The average polytropic index of the expansion process can be calculated by setting the total expansion work (Eq. (9)) equal to the equivalent average expansion work (Eq. (11)).

$$W_{\text{avg,E}} = \frac{n_{\text{avg}}}{n_{\text{avg}} - 1} V_{1E} P_{\text{CR}}^{\frac{1}{n_{\text{avg}}}} \left( P_{\text{CR}}^{\frac{n_{\text{avg}} - 1}{n_{\text{avg}}}}^{\frac{n_{\text{avg}} - 1}{n_{\text{avg}}}} - P_{\text{atm}}^{\frac{n_{\text{avg}} - 1}{n_{\text{avg}}}} \right)$$
(11)

The average polytropic index can then be solved for.

The isothermal roundtrip efficiency ( $\eta_{\rm RT}$ ) for a paired set of compression and expansion processes can be calculated as

$$\eta_{\rm RT} = \eta_{\rm iso,C} * \eta_{\rm iso,E} = -\frac{\int_{V_{\rm IE}}^{V_{\rm 2E}} (P - P_{\rm atm}) dV + (P_{\rm CR} - P_{\rm atm}) V_{\rm IE}}{\int_{V_{\rm CC}}^{V_{\rm 2C}} (P - P_{\rm atm}) dV - (P_{\rm R} - P_{\rm atm}) V_{\rm 2C}}$$
(12)

This roundtrip efficiency only accounts for the losses in the compression and expansion processes and does not include valve losses, mechanical losses, or storage losses. It assumes constant pressure storage and the ability to keep the output pressure constant during the discharge process. Therefore, to get a full view of the overall roundtrip efficiency of a CAES system, this isothermal roundtrip efficiency should be combined with other roundtrip system losses, such as storage losses, pump efficiency, pipe friction, and valve losses.

Mass loading (ML) is the ratio of droplet mass ( $m_d$ ) currently aloft in the chamber to air mass ( $m_a$ ) in the chamber at any given time.

$$ML = \frac{m_{\rm d}}{m_{\rm a}} \tag{13}$$

Other forms of mass loading are useful to define since the instantaneous mass loading defined above will vary over the course of a process. The total mass loading ( $ML_{\rm tot}$ ) is defined herein as the total mass of droplets in contact with air during the process, divided by the air mass. This includes both the droplets already in the chamber when the compression or expansion process starts ( $m_{\rm d,1}$ ) from the draw-in process, and those injected during the compression or expansion process ( $m_{\rm d,1\rightarrow2}$ ).

$$ML_{\text{tot}} = \frac{\left(m_{\text{d},1} + m_{\text{d},1 \to 2}\right)}{m_{\text{a}}} \tag{14}$$

When considering a combined compression and expansion process, the roundtrip mass loading  $(ML_{\rm RT})$  is defined as the average of the two total mass loadings.

$$ML_{\rm RT} = \frac{ML_{\rm tot,C} + ML_{\rm tot,E}}{2} \tag{15}$$

The Crowe number (Cr) was proposed by Simpson et al. [18] to relate the droplet thermal response time ( $\tau_{\rm T}$ ) to the fluid domain time scale ( $\tau_{\rm D}$ ). A similar relationship between a thermal time constant and droplet fall time was proposed by Odukomaiya et al. [7]. It can be calculated before simulations as follows, where the isothermal process time is the same for either compression or expansion. For all compression processes,  $L_1 = L_C = L_{\rm cyl}$ , and for an isothermal process,  $L_{2,\rm iso} = L_{\rm cyl}/PR$ ; for all expansion processes,  $L_1 = L_E = L_{\rm cyl}/PR$ , and for an isothermal expansion process,  $L_{2,\rm iso} = L_{\rm cyl}$ .

$$Cr = \frac{\text{thermal response time}}{\text{domain time scale}} = \frac{\tau_{\text{T}}}{\tau_{\text{D}}}$$
 (16a)

$$Cr = \frac{\rho_{\rm d}d^2c_s}{6Nuk_a} \left( \frac{1}{t_{\rm full}} + \frac{1}{t_{\rm iso}} \right)$$
 (16b)

$$t_{\text{fall}} = \frac{\frac{L_1 + L_{2,\text{iso}}}{2}}{w_{\text{term}}} = \frac{\left(1 + \frac{1}{PR}\right)L_{\text{cyl}}}{2 \times w_{\text{term}}}$$
 (16c)

$$t_{\rm iso} = \frac{\left|L_1 - L_{2,\rm iso}\right|}{U_{\rm piston}} = \frac{\left(1 - \frac{1}{PR}\right)L_{\rm cyl}}{U_{\rm piston}} \tag{16d}$$

When evaluating how well the droplets are able to improve the compression or expansion processes, the thermal equilibrium limit (defined in Simpson et al. [18], based on Ref. [28]) can be used as a lower limit on polytropic indices.

$$n_{\rm m,eq} = \frac{m_{\rm a}c_p + m_{\rm d}c_s}{m_{\rm a}c_v + m_{\rm d}c_s} = \frac{c_p + c_s \, ML_{\rm tot}}{c_v + c_s \, ML_{\rm tot}}$$
(17)

The thermal equilibrium limit is the polytropic index that would be reached if droplets and air were always in thermal equilibrium in the limit of infinitely fast heat transfer with infinitely small droplets. Therefore, this limit is the lowest polytropic index expected for a mixture of droplets and air without heat transfer to the environment. It is calculated herein using the total injected mass loading.

#### 2.3. Parametric analysis

A sweep of compression simulations and a matching sweep of expansion simulations were run based on the parameters given in Table 1. Herein, "matched" pairs of compression and expansion simulations are ones where the total cylinder length and diameter, piston speed, target pressure ratio, spray flow rate, and spray droplet diameter are all the same. Holding the spray droplet diameter and flow rate constant is representative of using the same nozzle and injection system for both compression and expansion processes, though it will not result in equivalent total mass loading for the matched compression and expansion processes.

The ranges of parameters attempt to capture a wide range of design options, while staying within the bounds of realistic processes and including the range of parameters used to validate the 1-D numerical method in Simpson et al. [18]. For example,  $U_{piston}=0.03~\text{m/s}$  is the piston speed from the experiments used to validate the 1-D method, but it is likely too slow for an energy storage process. At the other extreme,  $U_{piston}=0.6~\text{m/s}$  is estimated to the maximum speed for a partially or fully liquid piston. For cylinder lengths, the experiments used to validate to 1-D method used a total length around 0.1 m, but longer pistons are predicted to increase the system efficiency, so the range was extended up to  $L_{\rm cyl}=0.5~\text{m}$ .

# 2.4. Spray work validation

In general, spray work depends on the overspray pressure ( $\Delta P$ ) and the spray flow rate ( $q_{\rm spray}$ ) (based on Ref. [23]).

$$W_{\text{spray}} = \int_0^{t_2} \Delta P \, q_{\text{spray}} \, dt \tag{18}$$

Spray is injected during the draw-in period and also during the

 $\begin{tabular}{ll} \textbf{Table 1}\\ \textbf{Parametric sweep parameters for compression and expansion sweeps with direct injection spray.} \end{tabular}$ 

Parameter	Units	Values	Count
d	μm	200, 150, 100, 50, 25	5
$L_{\mathrm{cyl}}$	m	0.1, 0.3, 0.5	3
$U_{ m piston}$	m/s	[0.03, 0.6] linear spacing	4
$q_{ m spray}$	L/s	[5e-4, 2e-2] linear spacing	8
PR	-	2, 6, 10	3
Total			1440

compression or expansion process from time t=0 to  $t=t_2$ . This spray work includes spray operations during compression and expansion portions. The spray work for compression should be added to the compression work to find the total input work, while the spray work for expansion should be subtracted from expansion work to find the net output work.

Experimental data reported in Patil et al. [15] provides information on compression work and spray work for a spray-cooled liquid piston compressor. These experiments were previously used to validate the 1-D compression model in Simpson et al. [18], within the margin of experimental error. Using the same method from Ref. [18], the 69 kPa (10 psi) and 482 kPa (70 psi) spray cases were simulated using the Sauter mean diameter of the spray distributions. The BETE spray nozzle used provided a polydisperse droplet distribution with a Sauter mean diameter of 487  $\mu m$  for 69 kPa and 117  $\mu m$  for 482 kPa.

The compression work and spray work are compared between reported experimental results and calculated simulation results in Table 2. The overspray pressure was set based on the given spray pressures of 69 kPa and 482 kPa, respectively. The simulation results are able to predict experimental work with <8 % error. Also note that the spray work only slightly increases the total work for the low spray case (69 kPa), but the spray work nearly doubles the total work for the high spray case (482 kPa).

# 2.5. Spray work parametric analysis

A model was needed to incorporate spray work for water droplets into simulations where the droplet diameter is specified but the overspray pressure is not known. As such, a model for overspray pressure was developed based on experimental results from the literature to estimate the spray work in a sweep of simulations. The relationship between droplet size, flow rate, and overspray pressure is highly complex and depends on nozzle type, chamber pressure, etc. Many relationships can be found in the literature [29], but most either require specific nozzle information or use fluids other than water. Since pressure-swirl nozzles were found by Qin et al. [30] to provide high flow rates for small drop size ( $<100~\mu m$ ) while avoiding spray-work losses due to aeration, the present study focused on these same type of nozzles.

Data published in Wang & Lefebvre [31] provides the good data for conditions relevant to these simulations (Fig. 2). In that paper, water sprays were analyzed and the Sauter mean diameter, flow rate, and overspray pressure were all reported. Wang & Lefebvre proposed an equation to predict the Sauter mean diameter of a spray, but it uses many additional terms like the spray cone angle and film thickness. These terms allow consideration of multiple spray nozzles and conditions; however, the present study sought a simplified relationship for a single nozzle in terms of water spray Sauter mean diameter. A surface was fit to the data [31] based on the following relationship for diameter, which can be rewritten for overspray pressure as

$$d = A^* q_{\text{spray}}^B ^* \Delta P^C \tag{19a}$$

**Table 2**Comparison of compression and spray work reported from Patil et al. [15] with simulation results.

	Exp. data	Sim. results	% error
69 kPa			
Comp. work	42.6 J	44.4 J	4 %
Comp. + spray work	43.7 J	45.6 J	4 %
482 kPa			
Comp. work	35.7 J	37.3 J	4 %
Comp. + spray work	63.9 J	68.5 J	7 %

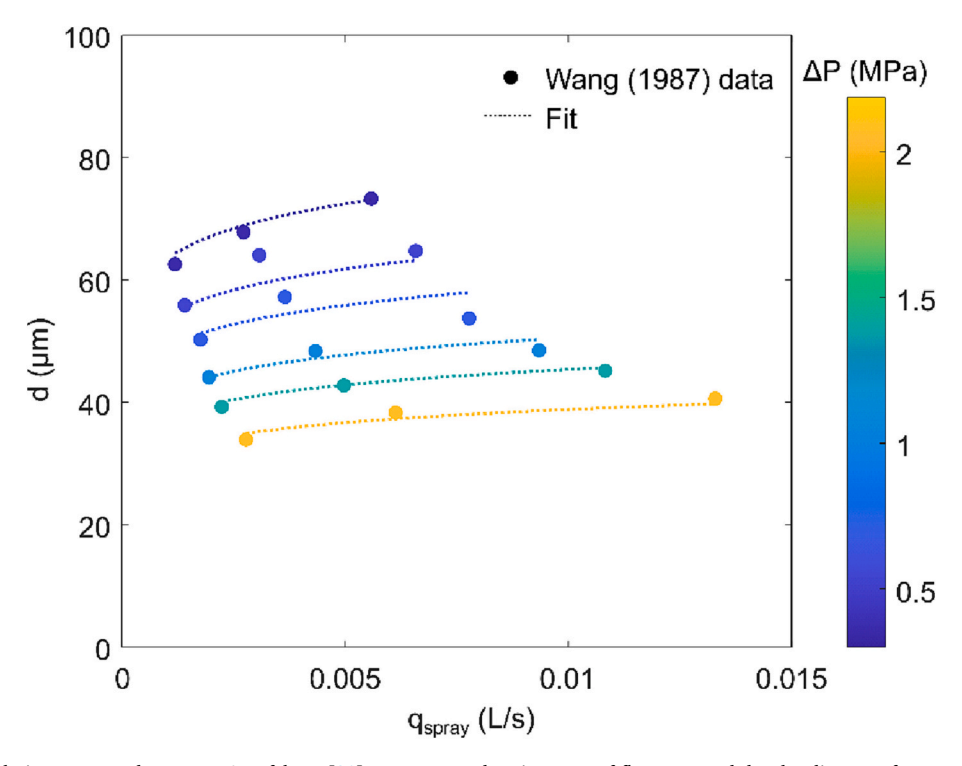


Fig. 2. Present fitted relation compared to Wang & Lefebvre [31] water spray data in terms of flow rate and droplet diameter for a set of overspray pressures.

$$\Delta P = \left(\frac{d}{A^* q_{\rm spray}^B}\right)^{\frac{1}{c}} \tag{19b}$$

The form of Eq. (19a) is similar to those reported in Ref. [29]; where C is generally between -0.25 and -0.47. Based on the experimental data, the coefficient values were adjusted to minimize error resulting in values of  $A=2.612\times10^4$ , B=0.082, and C=-0.383, with  $R^2=0.97$ . The results with these fitted coefficients are compared to the experimental data in Fig. 2 for six different overspray conditions. Increasing flow rate slightly increases droplet diameter but increasing overspray pressure has a much stronger effect on droplet diameter.

Using the spray pressure equation developed above, a sweep of simulations was run including spray work for conditions within or near the experimentally-based conditions of Fig. 2. Thus, it is a more concentrated and physically realistic sweep (assuming use of pressure-swirl nozzles) than the first one outlined in Table 1. The parameters for the sweep with spray work are given in Table 3. Additionally, the length of the cylinder was extended, to seek higher roundtrip efficiencies, as discussed in Section 3.3.

# 3. Results and discussion

# 3.1. Time-series results

The simulations (using the model described in Section 2.1) are considered in term of the time variations within a compression or

**Table 3**Parametric sweep including spray work parameters, for compression and expansion simulations.

Parameter	Units	Values	Count
d <sub>p</sub>	μm	80, 50, 30	3
$L_{ m cyl}$	m	[0.1, 1] linear spacing	4
U <sub>piston</sub>	m/s	[0.05, 0.5] linear spacing	5
q <sub>spray</sub>	L/s	[1e-3, 1.5e-2] linear spacing	4
PR	-	2, 6, 10	3
Total			720

expansion process to investigate the thermo-fluid physics. Figs. 3 and 4 show one example set of matching compression and expansion simulations with the following parameters: D=0.1 m,  $L_{\rm cyl}=0.3$  m, PR=10,  $U_{\rm piston}=0.2$  m/s, d=100  $\mu$ m,  $q_{\rm spray}=5\times10^{-3}$  L/s, and Cr=0.23.

In Fig. 3, the log-log pressure-volume changes are shown for the spray-based simulation as well as for an isothermal and an adiabatic process for this pressure ratio. The total work in or out of the process for the spray-based simulation is shaded in light blue. Ideally, the process would approach the isothermal curve for both the compression and expansion processes. Similar to results found in liquid piston experiments [13] and simulations [6], the compression simulation gives a relatively straight line (on a log-log plot) and is initially favorably close to isothermal limit, while the expansion simulation favorably curves towards the isothermal limit later in the simulation. The shaded pink region denotes the time spent between PR = 5 and PR = 10, which is more than half the process in terms of work in or out of the system. Thus, while the expansion process seen in Fig. 3 only appears to diverge slightly from the isothermal curve, the result is large because the majority of the expansion work is occurring during that phase. The times during the compression and expansion processes when the simulation diverges from the isothermal curve may be due to a combination of when the majority of the work is flowing in/out the process and when the instantaneous mass loading is lowest.

To further investigate the differences, the instantaneous mass loading, droplet and air temperatures, and polytropic index are plotted over time for the same example compression and expansion processes in Fig. 4. Note that the mass loading does not start at zero because spray is injected during the draw-in process when air is brought into the cylinder. The draw-in process takes longer before the compression process because the piston moves further, and thus the starting mass loading is higher for the compression process than the expansion process (as seen in Fig. 1). Again, the first/last 50 % of the expansion/compression process is shaded pink. This region is a small fraction of the process in time but accounts for a large fraction of the total work and results in large changes in air and droplet temperature.

The instantaneous polytropic index and temperature curves seen here align with previous work in the literature that has shown variable

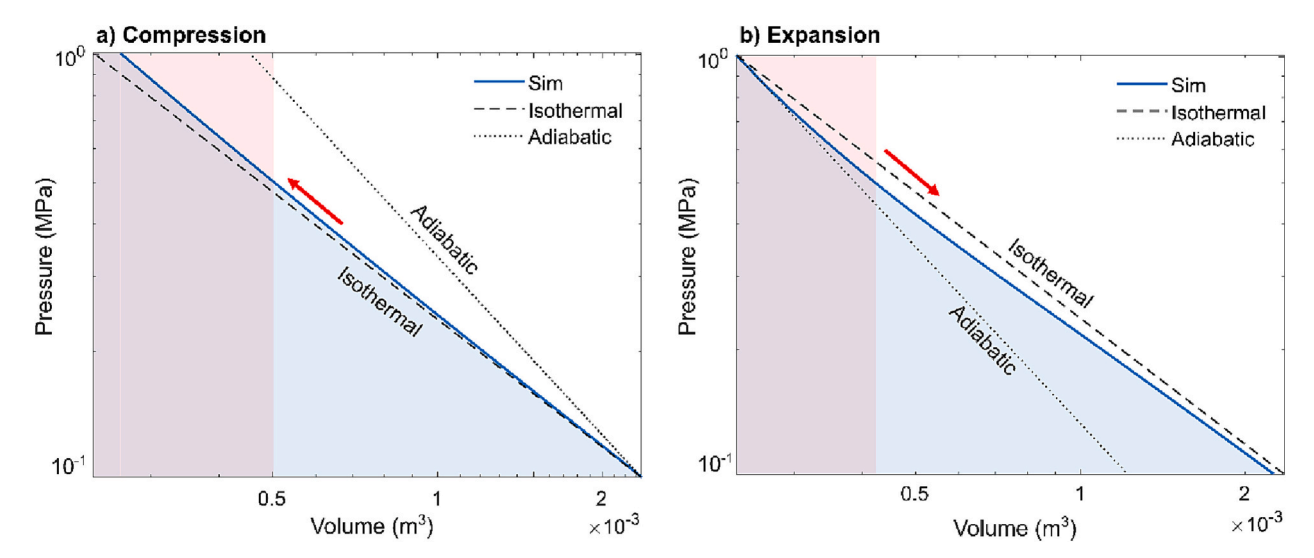


Fig. 3. (a-b). Pressure-volume curves for 1-D spray simulations of compression and expansion, compared to isothermal and adiabatic curves. The shaded blue region denotes the work in or out of an example pair of spray-based simulation processes (which include finite heat transfer), while the shaded pink region denotes the first/last 50 % of the expansion/compression process. (For interpretation of the references to color in this figure legend, the reader is referred to the web version of this article.)

heat transfer coefficients during the compression process [4]. However, the variations in Fig. 4f are especially interesting (and not previously discussed in the literature). During the initial time when most of the work is extracted (pink shaded region), the polytropic index is significantly above unity indicating some thermal losses. This period corresponds with significant differences between the drop and air temperature as seen in Fig. 4d, which results because the temperature decrease due to expansion is faster than any temperature warming due to droplet heat transfer. In contrast, the remaining expansion process spends most of its time below a polytropic index of 1. This is because the temperature rise due to heat transfer from the droplets is faster than the temperature decrease that would occur due to expansion. Notably, the resultant equivalent average polytropic index is weighted by the expansion work in the earlier period and thus remains above 1 as expected. However, these results show that the instantaneous polytropic index can vary dramatically and can be both greater and less than unity. This result is reflected by the trends in Fig. 3b for which the initial portion shows a pressure-volume downward slope that is close to adiabatic, while the remaining portion shows a larger slope than the isothermal slope. However, the initial portion has a stronger contribution, so the net effect is an average slope that is below isothermal slope so that the net work extracted is less than that for a purely isothermal process.

#### 3.2. Compression, expansion, and roundtrip efficiency

The results of the parametric analysis defined by Table 1 (total of 2880 simulated cases) are presented below, for compression and expansion without accounting for spray work. The polytropic index (n) is plotted against total mass loading ( $ML_{\rm tot}$ ) in Fig. 5. In both cases, the polytropic index tends to decrease and approach the thermal equilibrium limit as mass loading increases and as the Crowe number decreases. As expected, the spray-based simulation performance does not exceed the thermal equilibrium performance (i.e., the n values do not drop below the equilibrium limit black line) but approaches the equilibrium limit when the Crowe number is small (much less than unity). The equilibrium limit only approaches the isothermal limit (n=1) for high mass loadings (much greater than unity) and this is also true for the simulations with small Crowe numbers. These trends were common for both compression and expansion.

In addition to the above commonalities, there are also differences

between expansion and compression. Notably, the expansion simulation polytropic indices do not approach as close to the thermal equilibrium limit as the compression cases. The increased polytropic index for expansion is particularly true for mass loadings less than unity and for high pressure ratios. High pressure ratios lead to longer compression and expansion times for a given piston speed which is favorable; however, for a fixed total mass loading, these longer times lead to lower initial mass loading at the critical start of the expansion process. Thus, the difference in instantaneous mass loadings between compression and expansion simulations during times of large temperature changes is likely the cause of the difference in polytropic indices, which is exaggerated at low total mass loading and high pressure as those are the least efficient cases. This aspect suggests that performance can be increased if the water spray flow rates are varied in time such that higher mass loadings would occur during the interval when most of the work interaction occurs.

To further investigate the compression and expansion differences, the mass loading and polytropic index can be seen in Fig. 6, where each circle represents one matched pair of compression and expansion simulations at the same pressure ratio, spray parameters, and piston parameters. The compression total mass loading is equal to or higher than the expansion mass loading for each pair of simulations (due to longer draw-in time for compression). Thus, expansion tends to have a lower total mass loading and higher polytropic index than compression for the same matched set up; in addition, for the same total mass loading, expansion still has a higher (worse) polytropic index than compression (as seen in Fig. 5). Therefore, a change to the design would be needed to reach an equivalent polytropic index for both the compression and expansion processes, such as increasing the spray flow rate during the expansion draw-in process or using premixing for the expansion process.

While the polytropic index tells us about the thermodynamics of the process, the isothermal efficiency is most useful to a CAES system designer. The expansion isothermal efficiency results are plotted in Fig. 7 as a function of total mass loading, for three different pressure ratios. A similar parametric sweep of compression simulation isothermal efficiencies is reported in Simpson et al. [18]. As expected, expansion efficiencies approach that of isothermal compression for increased mass loading and for reduced Crowe number. The effect of Crowe number becomes more pronounced at large pressure ratios. Again, it can be seen that the spray-based expansions at higher pressure ratios are not able to reach the thermal equilibrium limit, even with small Crowe numbers,

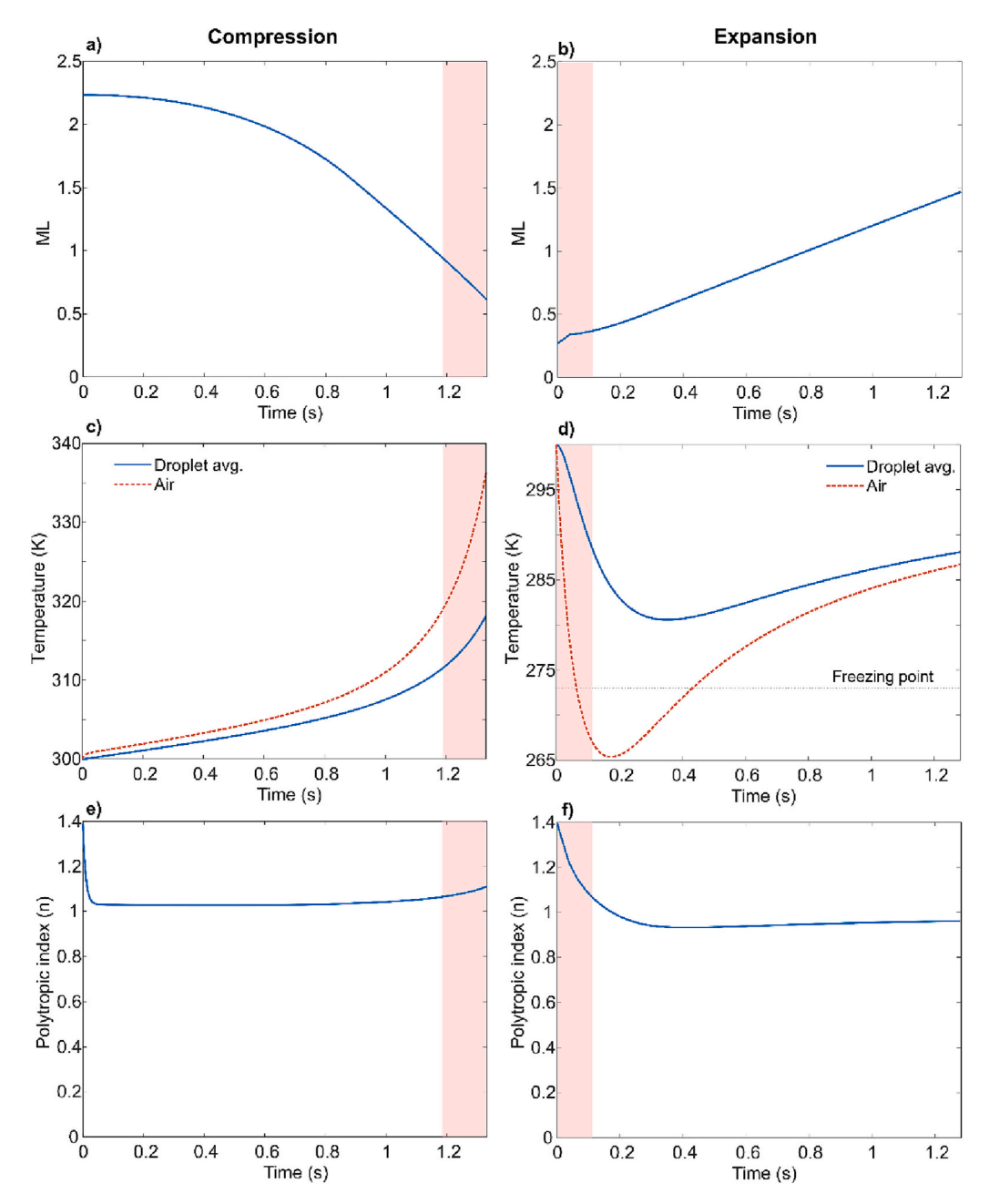


Fig. 4. (a–f). Time series results from 1-D model for an example matched pair of compression and expansion simulations at PR = 10, where the pink-shaded region denotes the last/first 50 % of the compression/expansion process.

and this is particularly true for the mass loadings around unity.

The results from the matched compression and expansion simulations are combined to calculate isothermal roundtrip efficiencies, plotted in Fig. 8. Every point in Fig. 8 represents a matched pair of compression and expansion simulations, with the isothermal roundtrip efficiency calculated with Eq. (14) and the roundtrip mass loading calculated with Eq. (13). For a pressure ratio of 2, the change in efficiency with mass loading and Crowe number is small. The efficiencies are all generally high, whereby isothermal roundtrip efficiency >95 % can be reached with  $ML_{\rm RT}>1$  for Cr<0.06, or with  $ML_{\rm RT}>10$  for Cr<4. For a pressure ratio of 10 (expected to be more practical for energy storage systems), the changes in efficiency with mass loading and Crowe number are more significant, consistent with Fig. 7. To reach a roundtrip efficiency of at least 95 %, the spray-based system must employ  $ML_{\rm RT}>6$  for Cr<0.02, which corresponds to relatively small drop sizes (e.g., 50  $\mu$ m in diameter). For larger drop sizes corresponding

to a criterion of Cr<0.77 (e.g., 150  $\mu m$  in diameter), the mass loading would need to be much larger ( $ML_{RT}>20$ ) to reach at least 95 % roundtrip efficiency.

In full-scale compressed air energy storage systems, it is expected that high pressure ratios (10:1 or even greater) would be used to increase the power to weight ratio of the system. To investigate potential efficiencies for such conditions, the highest isothermal roundtrip efficiency cases at a pressure ratio of 10 for each droplet diameter are given in Table 4, without spray work included. For these cases, the highest efficiency cases are the highest mass loading cases, with slow compression speed and high spray flow rates. Notably, isothermal roundtrip efficiencies of  $>\!99$  % are readily obtained with droplet sizes below 100  $\mu$ m, if spray-work is neglected.

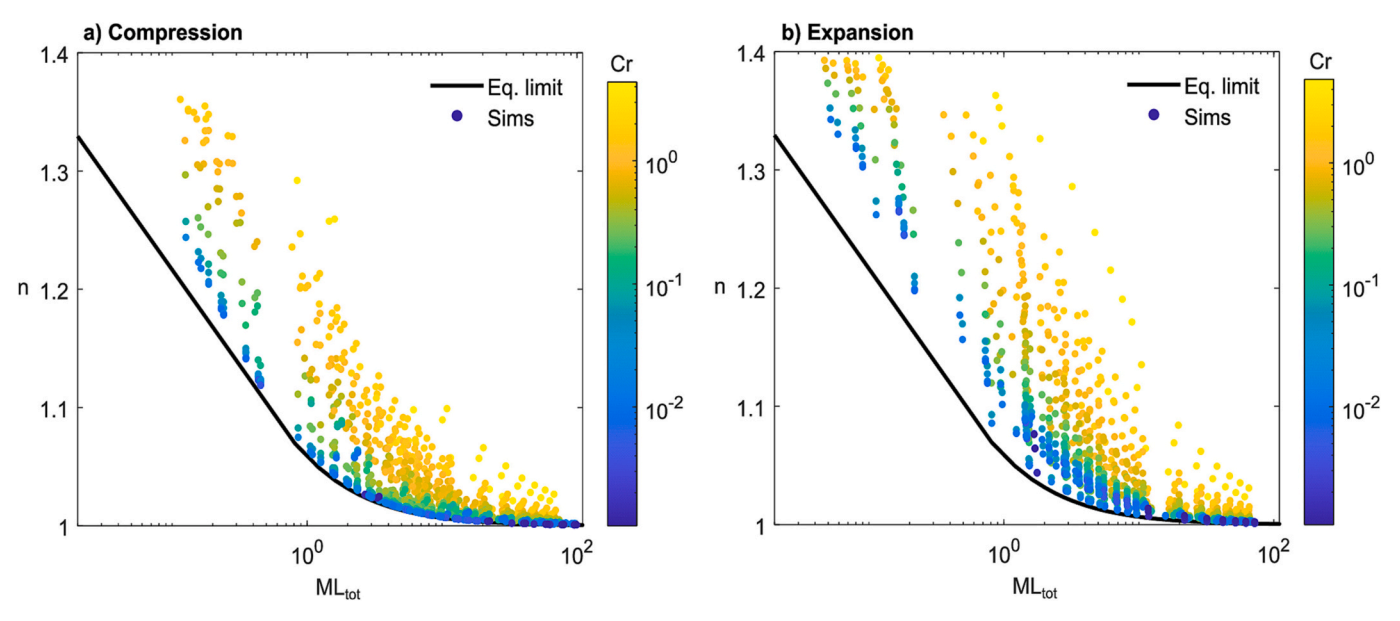


**Fig. 5.** Polytropic index (n) versus total mass loading ( $ML_{tot}$ ) colored by Crowe number (Cr) where the thermal equilibrium limit is plotted in black (while n = 1 is isothermal limit and n = 1.4 is adiabatic limit) for: a) compression and b) expansion.

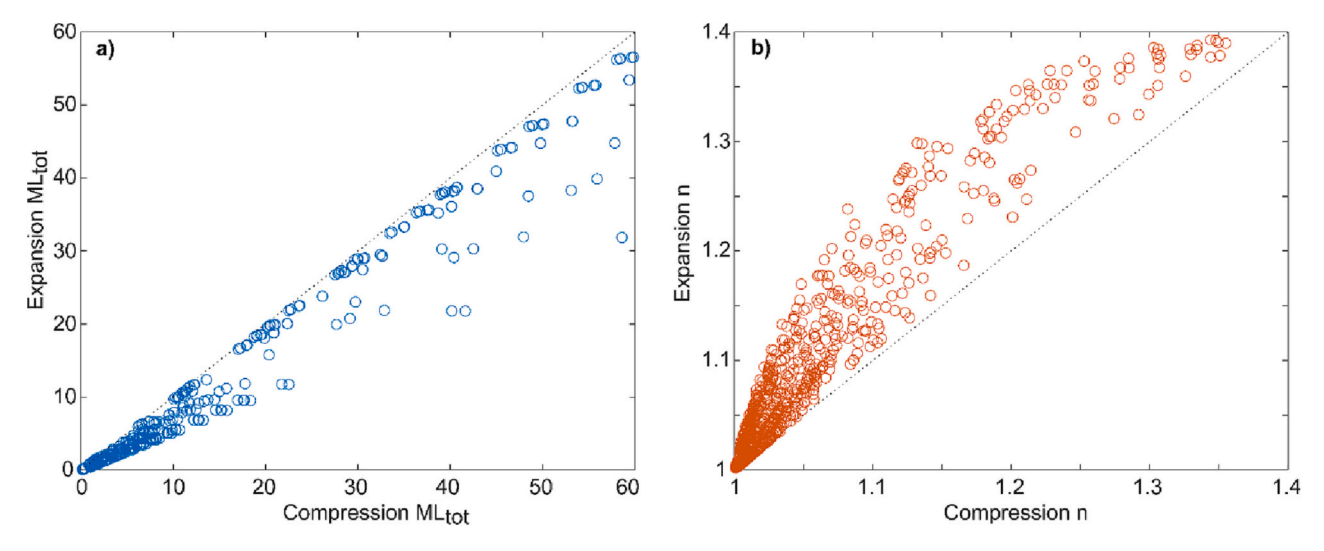


Fig. 6. Comparing compression and expansion matched simulations a) total mass loading and b) polytropic index. Each circle represents a matched pair of compression and expansion simulations.

# 3.3. Spray work

The second set of compression and expansion simulations includes spray work for the parameters given in Table 3. The resulting isothermal efficiencies for the compression and expansion simulations are shown in Fig. 9, where pressure ratios are distinguished with different colors and droplet diameters are distinguished with different shapes. Unlike the efficiencies in Figs. 7 and 8, these curves have a parabola-like trend where the efficiency first increases with mass loading and then decreases at high mass loadings, with a peak at intermediate mass loadings. For a given droplet size and pressure ratio, the results indicate an optimal mass loading (based on highest efficiency) that varies based on pressure ratio and droplet size. Also note that at low mass loadings, the highest efficiency processes are those with a pressure ratio of 2 (blue symbols), while at high mass loadings, the highest efficiency processes have droplet diameters of 80  $\mu$ m (triangular symbols).

Finally, the spray work compression and expansion simulations were paired to find the roundtrip efficiencies, plotted in Fig. 10. The previous

trend observed without spray work, where low Crowe numbers approach the thermal equilibrium limit, is again seen for low mass loadings with spray work. However, at higher mass loading the Crowe number trend reverses as the inclusion of spray work lowers the isothermal roundtrip efficiency. Thus, Crowe number becomes less important as a design parameter at higher mass loadings. As a result, roundtrip efficiencies tend to peak around a roundtrip mass loading of  $5 < ML_{RT} < 15$ , and then decline as the additional spray work outweighs the additional temperature benefits of the spray. This is particularly true at high mass loadings for the smaller drops, which give small Crowe numbers but require higher spray over-pressures. Similar results are seen in the literature, where increasing spray pressure can decrease compression efficiency [15,21,23]. As such, spray work should be generally included in the evaluation of droplet heat transfer systems with significant mass loadings (greater than unity) due to the potential adverse effect on efficiency.

To further demonstrate and quantify the above conclusions regarding spray work, the highest isothermal roundtrip efficiencies

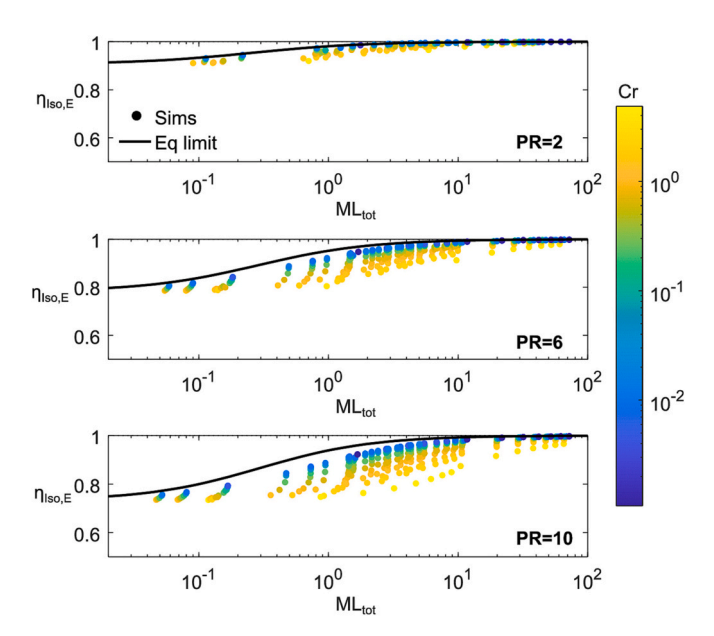


**Fig. 7.** Expansion simulations isothermal efficiency vs total mass loading, separated by pressure ratio and colored by Crowe number. Thermal equilibrium limit as black line upper limit.

including spray work for a pressure ratio of 10 for a given droplet size are listed in Table 5 for the parametric sweep of Fig. 10. Contrary to the results shown in Table 4, here the highest efficiency cases are those with moderate mass loadings. This is because the highest isothermal roundtrip efficiencies represent balances between spray work losses and temperature abatement improvements from the spray heat transfer. Additionally, the highest efficiencies expected with spray work are noticeably lower than those expected without accounting for spray work, where the differences are especially acute at small drop sizes. The highest efficiency cases resulted from the largest droplets of  $80\ \mu m$ , due to their low injection work relative to the smaller droplets. For these droplets sizes, long cylinder lengths and medium-speed piston motion tend to result in the highest efficiency. This is attributed to conditions that allow a low Crowe number (which allows more time for heat transfer to occur) while avoiding large mass loading and small drops (which use too much spray work). The cylinder length was further extended to see if an ideal length could be found, but the highest

**Table 4**Highest isothermal roundtrip efficiency cases for pressure ratio of 10 for each droplet size without spray work.

d (μm)	$q_{ m spray}$ (L/s)	$L_{\mathrm{cyl}}$ (m)	$U_{\rm piston}~({ m m/s})$	Cr	$\mathrm{ML}_{\mathrm{RT}}$	$\eta_{\mathrm{RT}}$
25	$1.44\times10^{-2}$	0.3	0.03	0.002	75.5	99.5 %
50	$2  imes 10^{-2}$	0.3	0.03	0.016	82.3	99.4 %
100	$2  imes 10^{-2}$	0.5	0.03	0.093	70.1	99.3 %
150	$2  imes 10^{-2}$	0.5	0.03	0.327	67.7	98.9 %
200	$2  imes 10^{-2}$	0.5	0.03	0.769	66.7	98.2 %

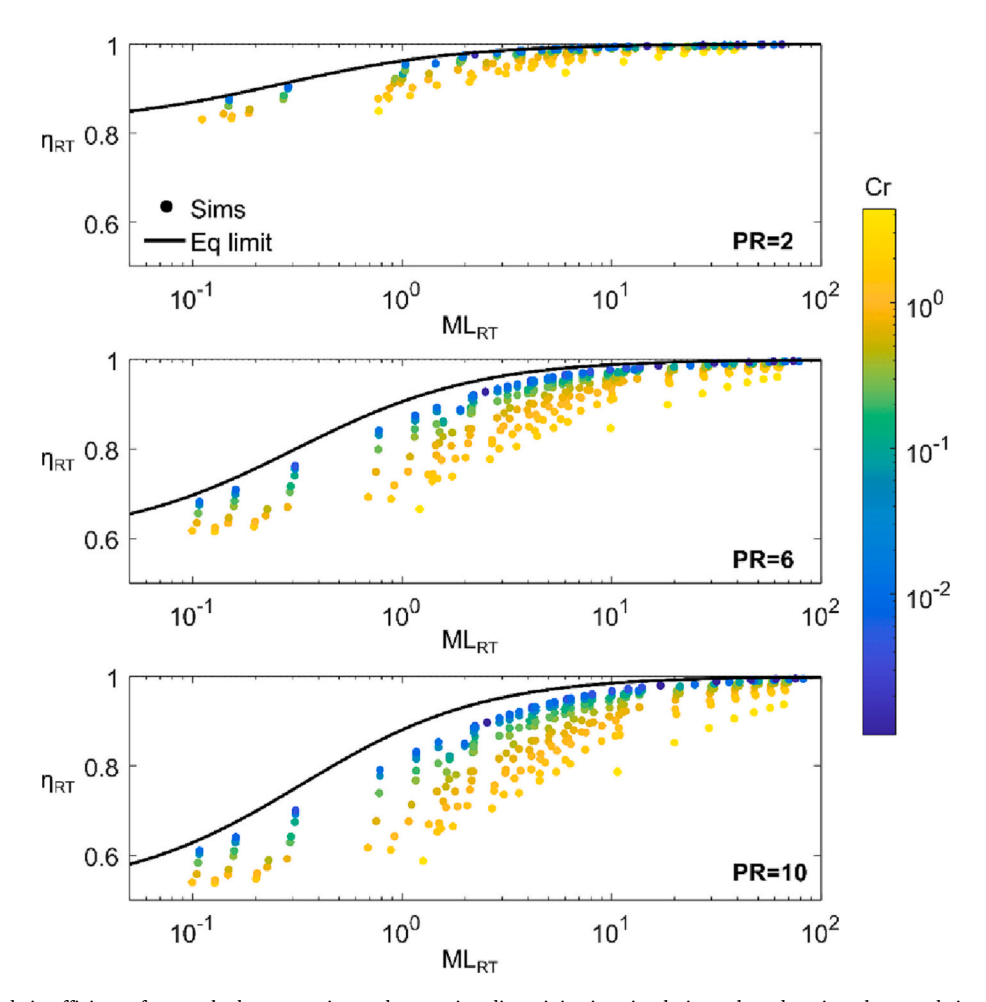


Fig. 8. Isothermal roundtrip efficiency for matched compression and expansion direct injection simulations plotted against the roundtrip mass loading, colored by Crowe number (Cr) and with the ideal equilibrium limit for roundtrip efficiency plotted in black.

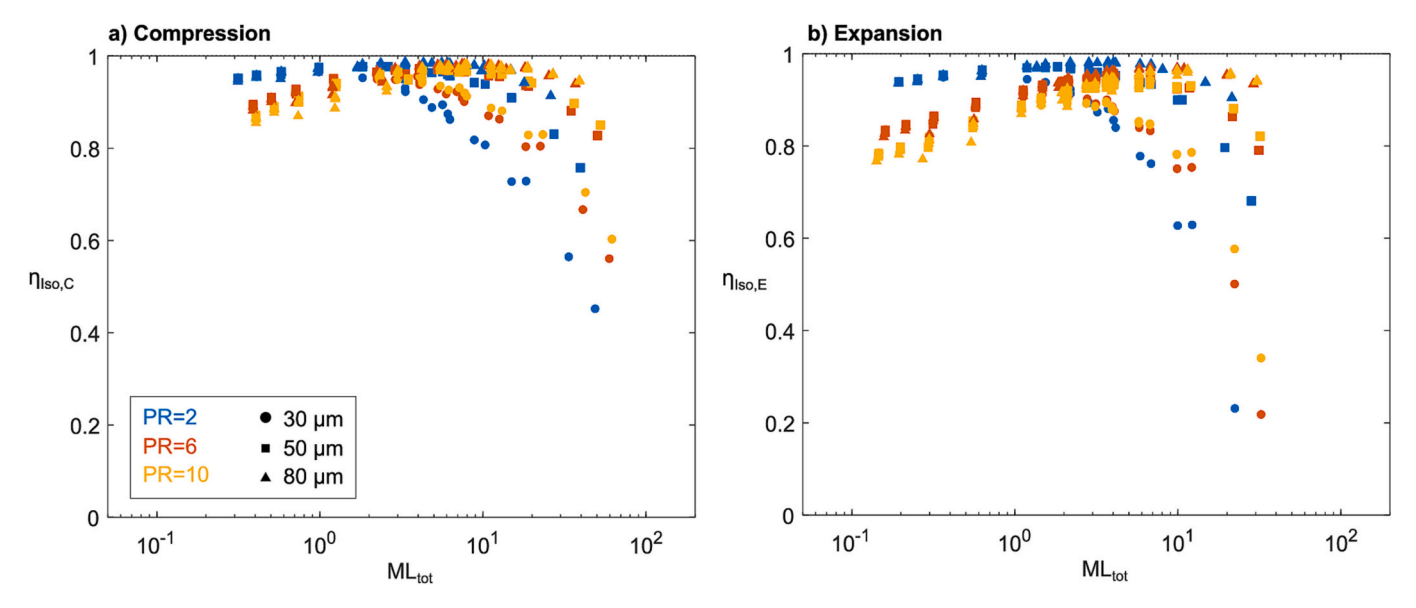


Fig. 9. (a–b). Isothermal efficiency for compression and expansion simulation sweeps including spray work. Pressure ratio (PR) shown in colors, droplet size shown in symbols. (For interpretation of the references to color in this figure legend, the reader is referred to the web version of this article.)

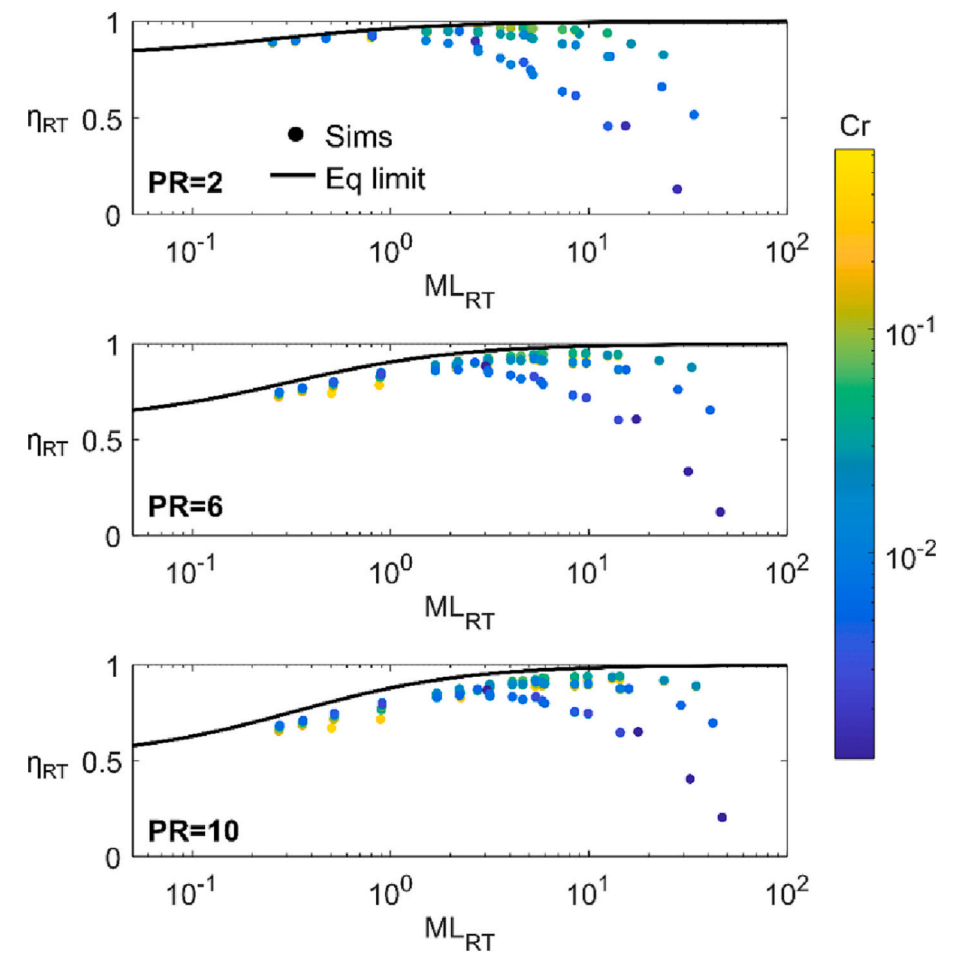


Fig. 10. Isothermal roundtrip efficiency for combined direct injection compression and expansion simulations including spray work, plotted against the roundtrip mass loading. Simulation results divided by pressure ratio (PR) and colored by Crowe number (Cr), where black line shows ideal thermal equilibrium limit for roundtrip efficiency without spray work.

**Table 5**Highest isothermal roundtrip efficiency cases for pressure ratio of 10 for each droplet size, including spray work.

d (μm)	q <sub>spray</sub> (L/s)	$L_{\mathrm{cyl}}$ (m)	U <sub>piston</sub> (m/s)	Cr	$ML_{RT}$	$\eta_{ m RT}$
30	$1  imes 10^{-3}$	1	0.05	0.001	3.1	86.9 %
50	$5.7  imes 10^{-3}$	1	0.1625	0.010	5.4	91.3 %
80	$1.5\times 10^{-2}$	1	0.1625	0.035	14.3	94.2 %

efficiency case continues to be the longest cylinder considered. However, these longer lengths are likely to increase the influence of multidimensional flow features, turbulence, and wall interactions, which are not included in the present study but which are expected to reduce the overall roundtrip efficiency.

# 4. Conclusions

Using a previously validated 1-D model for compression and expansion with spray injection, a parametric analysis of compression and expansion simulations was completed to better understand the thermal-fluid physics and roundtrip isothermal efficiency of a CAES system. Time-series results from simulations show that compression and expansion processes are not identical and have different polytropic index and temperature trends. Notably, the instantaneous polytropic index varies significantly during each process, which is not captured by only looking at the average polytropic index.

For both compression and expansion, average polytropic index of the process decreases and approaches isothermal with increasing mass loading and decreasing Crowe number. The expansion simulation polytropic indices do not approach as close to the thermal equilibrium limit as the compression cases, particularly for mass loadings less than unity and for high pressure ratios, which may be due in part to the timing of the mass loading. For the same process conditions, expansion cases have equal or lower total mass loading than compression cases, and equal or higher polytropic indices than compression cases.

Combining results from matched compression and expansion simulations excluding spray work with the same pressure ratio, drop size, and piston parameters, the highest isothermal roundtrip efficiency cases are those with the highest mass loading cases, with slow compression speed and high spray flow rates. A spray-based system can reach an isothermal roundtrip efficiency >95 % with a pressure ratio of 10 with  $ML_{\rm RT}>6$  for Cr<0.02, which corresponds to relatively small drop sizes.

A second smaller set of compression and expansion simulations were run including spray work, using a relationship fitted to experimental spray data. For validation, compression work and spray work from simulations were compared to experimental data, and predicted work with <8~% error.

When accounting for spray work, the highest roundtrip efficiency cases are those with moderate mass loadings and piston speed and long cylinder length. Isothermal roundtrip efficiencies tend to peak around a mass loading of  $5 < ML_{RT} < 15$ , and then decline as the additional spray work outweighs the additional temperature benefits of the spray and larger droplets are preferred. The highest isothermal roundtrip efficiency for a pressure ratio of 10 is 94.2 % with the largest droplets (80  $\mu$ m) and  $ML_{RT} = 14$ .

Some important design trade-offs for a high efficiency compression system can be informed from this study. For a given spray configuration, increasing process time via a longer cylinder and slower piston motion increases the isothermal efficiency. For a given piston and compression configuration, reduced droplet size and increased flow rate increases roundtrip efficiency when ML < 1, and reduced droplet size and increased flow rate must be balanced with increasing spray work to find the ideal roundtrip efficiency when ML > 1. For any given system, Crowe number is a driving factor for increasing isothermal efficiency for ML < 1, but Crowe number is no longer the sole factor at higher mass loadings and instead the Crowe number effect must be weighed against

the impact of high spray work.

Given the potentially large negative effect of spray work on isothermal efficiency, spray work should be included designs with significant mass loadings (e.g. greater than unity) due to the potential adverse effect on efficiency, and future work is recommended to implement a universal spray work equation to capture this effect in a larger variety of conditions. Additionally, isothermal efficiency may be increased by considering pre-mixed injection of droplets for expansion to increase the mass loading at the beginning of the expansion process, when the most work is extracted. The work herein using relatively small cylinders may be expanded in the future to design high-power systems with larger cylinder lengths on the scale of 1–5 m (for liquid pistons). Further investigation is recommended to consider effects of polydisperse droplet size distributions, multi-dimensionality, turbulence, wall-interactions, and droplet dynamics, and to investigate high-efficiency cases with experiments.

# CRediT authorship contribution statement

**Juliet G. Simpson:** Conceptualization, Methodology, Software, Formal analysis, Writing – original draft. **Chao Qin:** Conceptualization, Methodology, Writing – review & editing. **Eric Loth:** Conceptualization, Methodology, Writing – review & editing.

# **Declaration of competing interest**

The authors declare that they have no known competing financial interests or personal relationships that could have appeared to influence the work reported in this paper.

# Data availability

Data will be made available on request.

# Acknowledgments

This work was supported by the National Science Foundation Graduate Research Fellowship Program under Grant No. 1842490. Any opinions, findings, and conclusions or recommendations expressed in this material are those of the authors and do not necessarily reflect the views of the National Science Foundation.

### References

- M. Jafari, A. Botterud, A. Sakti, Decarbonizing power systems: a critical review of the role of energy storage, Renew. Sust. Energ. Rev. 158 (2022), 112077, https://doi.org/10.1016/j.rser.2022.112077.
- [2] J.A. Bennett, J.G. Simpson, C. Qin, R. Fittro, G.M. Koenig, A.F. Clarens, et al., Techno-economic analysis of offshore isothermal compressed air energy storage in saline aquifers co-located with wind power, Appl. Energy 303 (2021), 117587, https://doi.org/10.1016/j.apenergy.2021.117587.
- [3] M. Heidari, D. Parra, M.K. Patel, Physical design, techno-economic analysis and optimization of distributed compressed air energy storage for renewable energy integration, J. Energy Storage 35 (2021), 102268, https://doi.org/10.1016/j. est.2021.102268.
- [4] J. Menéndez, J.M. Fernández-Oro, M. Galdo, L. Álvarez, A. Bernardo-Sánchez, Numerical investigation of underground reservoirs in compressed air energy storage systems considering different operating conditions: influence of thermodynamic performance on the energy balance and round-trip efficiency, J. Energy Storage 46 (2022), 103816, https://doi.org/10.1016/j.est.2021.103816.
- [5] J. Mouli-Castillo, M. Wilkinson, D. Mignard, C. McDermott, R.S. Haszeldine, Z. K. Shipton, Inter-seasonal compressed-air energy storage using saline aquifers, Nat. Energy 4 (2019) 131–139, https://doi.org/10.1038/s41560-018-0311-0.
- [6] S. Hu, W. Xu, M. Cai, G. Jia, Energy efficiency and power density analysis of a tube array liquid piston air compressor/expander for compressed air energy storage, J. Energy Storage 55 (2022), 105674, https://doi.org/10.1016/j.est.2022.105674.
- [7] A. Odukomaiya, A. Abu-Heiba, K.R. Gluesenkamp, O. Abdelaziz, R.K. Jackson, C. Daniel, et al., Thermal analysis of near-isothermal compressed gas energy storage system, Appl. Energy 179 (2016) 948–960, https://doi.org/10.1016/j. apenergy.2016.07.059.

- [8] H. Chen, Thermodynamic analysis of an open type isothermal compressed air energy storage system based on hydraulic pump/turbine and spray cooling, Energy Convers. Manag. 13 (2020).
- [9] T. Neu, A. Subrenat, Experimental investigation of internal air flow during slow piston compression into isothermal compressed air energy storage, J. Energy Storage 38 (2021), 102532, https://doi.org/10.1016/j.est.2021.102532.
- [10] E.M. Gouda, Y. Fan, M. Benaouicha, T. Neu, L. Luo, Review on liquid piston technology for compressed air energy storage, J. Energy Storage 43 (2021), 103111, https://doi.org/10.1016/j.est.2021.103111.
- [11] M. Khaljani, A. Vennard, J. Harrison, D. Surplus, A. Murphy, Y. Mahmoudi, Experimental and modelling analysis of efficiency enhancement in a liquid piston gas compressor using metal plate inserts for compressed air energy storage application, J. Energy Storage 43 (2021), 103240, https://doi.org/10.1016/j. est.2021.103240
- [12] V.C. Patil, J. Liu, P.I. Ro, Efficiency improvement of liquid piston compressor using metal wire mesh for near-isothermal compressed air energy storage application, J. Energy Storage 28 (2020), 101226, https://doi.org/10.1016/j.est.2020.101226.
- [13] J. Wieberdink, P.Y. Li, T.W. Simon, J.D. Van de Ven, Effects of porous media insert on the efficiency and power density of a high pressure (210 bar) liquid piston air compressor/expander – an experimental study, Appl. Energy 212 (2018) 1025–1037, https://doi.org/10.1016/j.apenergy.2017.12.093.
- [14] B. Yan, J. Wieberdink, F. Shirazi, P.Y. Li, T.W. Simon, J.D. Van de Ven, Experimental study of heat transfer enhancement in a liquid piston compressor/ expander using porous media inserts, Appl. Energy 154 (2015) 40–50, https://doi. org/10.1016/j.apenergy.2015.04.106.
- [15] V.C. Patil, P. Acharya, P.I. Ro, Experimental investigation of water spray injection in liquid piston for near-isothermal compression, Appl. Energy 259 (2020), 114182, https://doi.org/10.1016/j.apenergy.2019.114182.
- [16] C. Qin, E. Loth, Liquid piston compression efficiency with droplet heat transfer, Appl. Energy 114 (2014) 539–550, https://doi.org/10.1016/j. apenergy.2013.10.005.
- [17] P. Sapin, M. Simpson, C. Kirmse, C.N. Markides, Dynamic modelling of water-droplet spray injection in reciprocating-piston compressors, in: Proceedings of ECOS 2018 The 31st International Conference On Efficiency, Cost, Optimization, Simulation And Environmental Impact Of Energy Systems, Guimaraes, Portugal, 2018, p. 12.

- [18] J.G. Simpson, C. Qin, E. Loth, Spray-cooled compression: theory and simulation, Appl. Therm. Eng. (2023), 120619, https://doi.org/10.1016/j. applthermaleng.2023.120619.
- [19] Q. Yu, X. Li, Y. Geng, X. Tan, Study on quasi-isothermal expansion process of compressed air based on spray heat transfer, Energy Rep. 8 (2022) 1995–2007, https://doi.org/10.1016/j.egyr.2022.01.019.
- [20] X. Zhang, Y. Xu, X. Zhou, Y. Zhang, W. Li, Z. Zuo, et al., A near-isothermal expander for isothermal compressed air energy storage system, Appl. Energy 225 (2018) 955–964, https://doi.org/10.1016/j.apenergy.2018.04.055.
- [21] J. Guanwei, X. Weiqing, C. Maolin, S. Yan, Micron-sized water spray-cooled quasiisothermal compression for compressed air energy storage, Exp. Thermal Fluid Sci. 96 (2018) 470–481, https://doi.org/10.1016/j.expthermflusci.2018.03.032.
- [22] B. Ahn, V.C. Patil, P.I. Ro, Effect of integrating metal wire mesh with spray injection for liquid piston gas compression, Energies 14 (2021) 3723, https://doi. org/10.3390/en14133723.
- [23] Q. Yu, Q. Wang, X. Tan, X. Li, Water spray heat transfer gas compression for compressed air energy system, Renew. Energy 179 (2021) 1106–1121, https://doi. org/10.1016/j.renene.2021.07.128.
- [24] E. Loth, Fluid Dynamics of Particles, Drops and Bubbles, Cambridge University Press, 2023
- [25] C. Qin, E. Loth, Simulation of spray direct injection for compressed air energy storage, Appl. Therm. Eng. 95 (2016) 24–34, https://doi.org/10.1016/j. applthermaleng.2015.11.008.
- [26] G. Jia, X. Nian, W. Xu, Y. Shi, M. Cai, Water-spray-cooled quasi-isothermal compression method: water-spray flow improvement, Entropy 23 (2021) 724, https://doi.org/10.3390/e23060724.
- [27] J.D. Van de Ven, P.Y. Li, Liquid piston gas compression, Appl. Energy 86 (2009) 2183–2191, https://doi.org/10.1016/j.apenergy.2008.12.001.
- [28] J. Kersey, E. Loth, D. Lankford, Effect of evaporating droplets on shock waves, AIAA J. 48 (2010) 1975–1986, https://doi.org/10.2514/1.J050162.
- [29] A.H. Lefebvre, V.G. McDonell, Atomization and Sprays, 2nd ed., CRC Press, 2017.
- [30] C. Qin, E. Loth, P. Li, T. Simon, J. Van de Ven, Spray-cooling concept for wind-based compressed air energy storage, J. Renew. Sustain. Energy 6 (2014), 043125, https://doi.org/10.1063/1.4893434.
- [31] X.F. Wang, A.H. Lefebvre, Mean drop sizes from pressure-swirl nozzles, J. Propuls. Power 3 (1987) 11–18, https://doi.org/10.2514/3.22946.